A nanochannel through a plasmonic antenna gap: an integrated device for single particle counting

Irene Fernandez-Cuesta, Melanie West, Enrica Montinaro, Adam Schwartzberg, and Stefano Cabrini

Supplementary Information

S1. Fabrication process and details

S1.1 Fluidic sample fabrication

The multifunctional micro/nano fluidic devices are fabricated following wafer-scale approaches, mainly based on nanoimprint lithography (NIL). A silicon stamp is made first by different lithographies and etching steps. A negative replica is then made using a polymer on a transparent substrate. And then, this negative replica is used to imprint the fluidic devices [1]. Each stamp (both, silicon and negative stamps) can be used multiple times. Then, a sacrificial layer and a gold layer are evaporated on the sample, to define the gold bowtie antennas just by shadow evaporation and lift off, so no additional lithography or alignment steps are necessary. Figure S 1 and Figure S 2 show the different steps of the fabrication process for the fluidic structures and the gold antenna respectively. A scheme and an image of a sample are shown for each step. And the details of each step explained next:

1. **SILICON STAMP.** A silicon stamp is first fabricated in a silicon wafer (Figure S 1.1). The nanochannels (30 nm wide, 30 nm deep) are defined by electron beam lithography (EBL) on PMMA. Adjacent to each nanochannels, two triangles (to make the gold antenna in later steps) are also defined in the same lithography step, so no alignment is necessary, what guarantees the best accuracy. After development, the nanostructures are etched by reactive ion etching (RIE). Some times, another EBL plus RIE step is done, to define transient nanochannels (400 nm wide, 400 nm deep), as can be seen in the devices in Figure S 4 and Figure S 5. Then, the microchannels are defined by photolithography followed again by RIE. Some of the devices have 2D or 3D tapered inlets connecting the micro and nanostructures. These can be fabricated by different methods: by gray-scale electron beam lithography plus thermal reflow [2], by focused ion beam milling, or by photolithography, depending on the desired final specifications as described in section S1.3 and shown in Figure S 4. The microchannels are defined by photolithography plus RIE. Finally, the stamp is coated with a monolayer of fluorosilanes by vapor deposition to improve the antiadhesive properties.

   The nanochannels are typically 30 nm wide, 30 nm deep, and several microns long. Depending on the specific application, their length can range from 4 μm up to 150 μm, as shown in Figure S 3 and Figure S 4. Nanochannels with smaller lateral dimensions can also be fabricated, although their use for fluidics becomes then very challenging. The triangles that will define the plasmonic antenna have sizes in the range of 100 nm by 100 nm. The microchannels are 20 μm wide, 1 or 2

μm deep. Several tens of nanochannels with their corresponding antennas are integrated in the same chip. And several chips (up to 16) are integrated within the same 4 inch silicon wafer stamp.

2. **POLYMER NEGATIVE TRANSPARENT STAMP.** A negative replica of the silicon stamp is made by UV nanoimprint lithography (UV-NIL) (Figure S 1.2). As active material, we use Ormostamp, a hybrid organic-inorganic polymer commercially available from microresist technology GmbH. A drop of the polymer is casted on the stamp, and pressed against a transparent substrate (typically a glass slide). The substrates are pressed together by hand, and exposed under a UV-lamp for 30 s, so the Ormostamp is cured, and they can be separated. The Ormostamp negative replica is coated with the fluorosilane. This is possible since the material contains silica groups, allowing for a homogeneous and stable fluorosilane monolayer. After silanization, the stamp can be used for nanoimprint lithography to make multiple fluidic devices.

3. **FLUIDIC DEVICES.** The all-**transparent polymeric fluidic devices** are made by direct UV-NIL using the negative stamp for imprinting (Figure S 1.3). A drop of Ormocomp (also a hybrid polymer from microresist technology GmbH) is cast on the stamp, manually pressed with a transparent substrate, and cured with UV light. After releasing the stamp, **all the complex multilevel, multidimensional fluidic circuitry is defined in the polymer, after just one curing step that takes 30 s**. There is flexibility for the substrate used - for most of the work presented here, we used glass slides or polycarbonate slides. But it is possible to use silicon, or a pre-patterned substrate. The final dimensions of the nanochannels, the triangles, and so the antenna gap do not differ from the original master stamp, as we observed by following the process step by step and shown elsewhere [1]. Also the microsctuctures maintain the quality, dimensions and surface smoothness along the process.

The fabrication of the stamp is the most critical part of the process, Once the stamp is fabricated, the fabrication of fluidic samples is straight forward, quick (needs just 30 seconds exposure), and does not require a pattern transfer, alignment, or post-processing, which saves time and greatly improves the reproducibility, especially for the smaller dimensions. The double replication scheme, starting from a silicon wafer and etching the structures is very convenient since we can achieve a perfectly flat surface on the polymer fluidic devices: the flat, upper part of the device maintains the smoothness of the surface of the original polished silicon wafer. This is crucial, since it is important to have ultraflat surface, to ensure a good bonding, for liquid sealing and to avoid leaking.

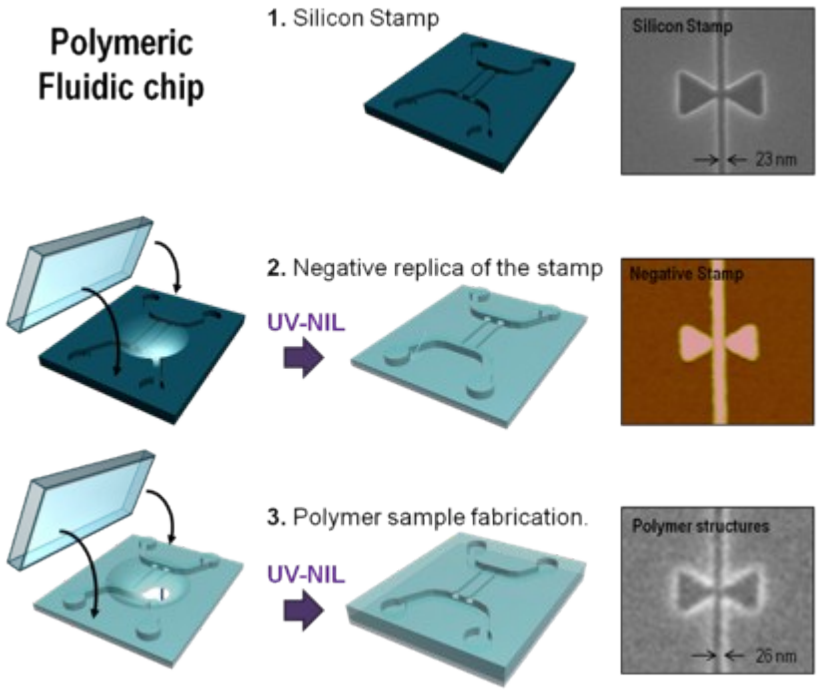

Figure S 1. Fabrication process I: fluidic device made by nanoimprint lithography. A silicon stamp (1) is first made by electron beam lithography (nanochannels and adjacent triangles) and optical lithography (microchannels) and etching. Tapered inlets might be also defined by FIB. The silicon stamp is replicated (2) on a polymer material (Ormostamp) by UV-nanoimprint lithography. After silanization, the negative stamp is used for imprinting (3) to make the fluidic samples. This step is 30 s long, and all the multilevel, multidimensional structures are patterned at the same time.

S1.2 Gold plasmonic nanoantenna fabrication

The bowtie antennas are then made of gold by shadow evaporation of a sacrificial layer, normal evaporation of gold, and lift off as shown in Figure S 2 and described next:

4 & 5. The polymer fluidic sample is loaded in an e-beam evaporator, tilted at 12º from the vertical axes. A 20 nm thick layer of chromium is evaporated. Since the sample is tilted, there is a shadow effect: the surface of the sample will be coated with the metal, but not the buried triangles adjacent to the nanochannel (which will define the antenna). This chromium layer will act as a sacrificial layer.

6. The sample is loaded again in the evaporator, but in a flat (standard) position. A 20 nm layer of gold is evaporated. The gold will cover completely the sample, including the triangles that were not coated in the previous step due to shadowing effects.

7. The sample is immersed in a wet chromium etch bath (based on ammonium ceric acid) and left with ultrasonic agitation for 15 minutes. Then, it is rinsed in water. This lift-off process removes all the metal from the sample's surface, except that inside the antenna triangles.

8. The resulting gold antennas are embedded in the polymer structures, perfectly aligned to the nanochannels (since they maintain the resolution from the e-beam lithography process) and are in the same plane, so the plasmonic hot spot is exactly inside the nanochannel. This process is wafer-scale, self align, and can be used to fabricate antennas made of pure gold (without adhesion layer).

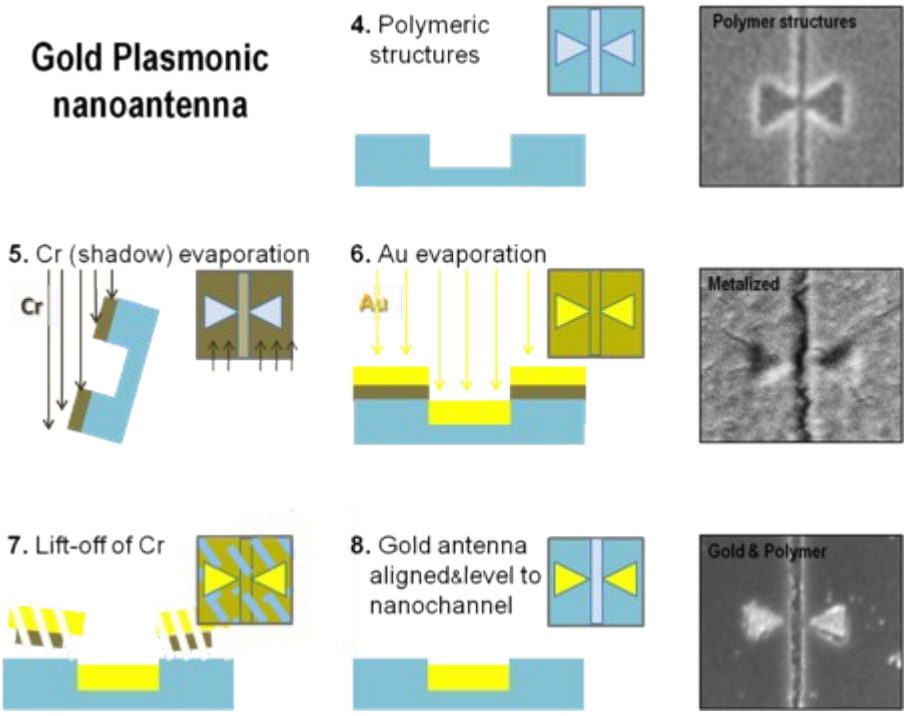

Figure S 2. Fabrication process II: integration of gold plasmonic antenna by evaporation and lift off. The polymer sample (4) is loaded in the evaporator tilted respect to the normal plane (5). A 20 nm thick layer of chromium is deposited, and shadow effects will prevent the triangles from metal coverage. A 20 nm thick gold layer (6) is then evaporated with the sample flat (standard position). A lift-off (7) in a chromium wet etch will remove the metal from everywhere, except inside the triangles, that will remain covered with pure gold (8). The whole process is wafer scale and self aligned.

To finalize the fabrication process, four holes (5 mm diameter) are drilled at the ends of the microchannels by sandblasting (in the glass substrates) or drilling (in the polycarbonate ones) to introduce liquid into the fluidic circuitry of the device. Then, the device is sealed by bonding to a glass coverslip. The final devices are several cm wide and long (2.5 cm x 7.5 cm, but these dimensions are flexible), easy to handle, and ready for plugging tubing, electrodes or connect to a fluidic holder for experiments.

S1.3 Types of devices

For this work, we fabricated different stamps, with different configurations, depending on the application envisioned for the device. We varied the number of channels per device, their distribution, their length, and the way they were connected to the microchannels (via transient nanochannels, tapered inlets, etc).

Nanochannel configuration

For example, we fabricated **devices with several channels, having different widths**, as shown in Figure S 3 (a-c) to test for example the passage of liquids and check how small their cross section can be while still allow the flow of liquids and molecules. These devices were also used to measure the elongation of DNA molecules inside nanochannels with dimensions. We also fabricated **devices with one or two identical nanochannels**, Figure S 3 (d-f), for repetitive measurements, to ensure that the measurements are performed in identical conditions.

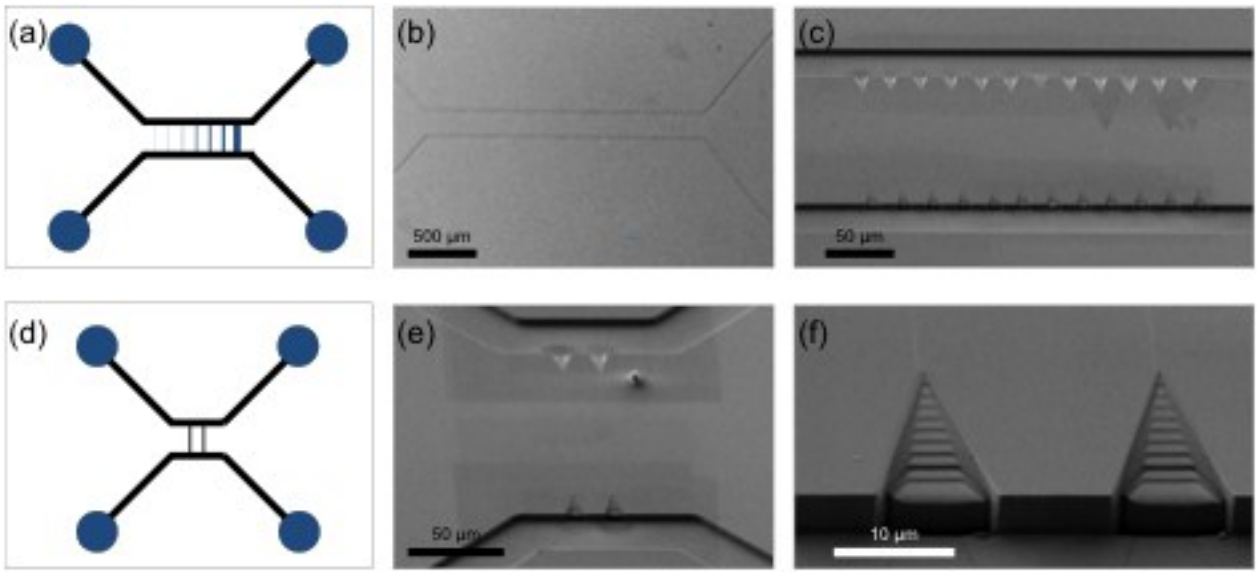

Figure S 3. Devices with several different nanochannels (a-c) were fabricated, as well as nanochannels with one or two identical nanochannels (d-f).

Inlet configuration

The fluidic layout of the devices was also optimized for the different measurements. The core, nanochannels with plasmonic nanoantenna, was maintained identical in all of them. But the way the nanochannels were interfaced was varied and tailored depending on the specific application. Several examples of layouts fabricated along this work are sketched in Figure S 4 (a), and shown in different SEM images in Figure S 4 (b-f), Figure S 3 and Figure S 5.

Short nanochannels (5 µm long) are useful for example for quick flow of particles or molecules, like quantum dots. An example of a device with several different short nanochannels interfaced with transient

nanochannels is shown in Figure S 5, where also the channels with different widths with their corresponding gold plasmonic antennas can be seen. A similar device was used for the measurements of the flow of quantum dots shown in the main text. We fabricated different types of transient inlet designs, symmetrical, where the antenna is in the center, in between the microchannels. But we also fabricated others with asymmetrical configurations (Figure S 4 (e,f)), placing the nanochannels with the antenna very close to one of the microchannels, to facilitate the flow, and study the effect of the transient inlets.

Long nanochannels are often necessary to measure the stretching of long DNA molecules. Some of these nanochannels, 150 um long, were directly connected to the microchannels. In others, 2D or 3D triangular inlets were used to facilitate the flow, as those shown in the two devices in Figure S 3.

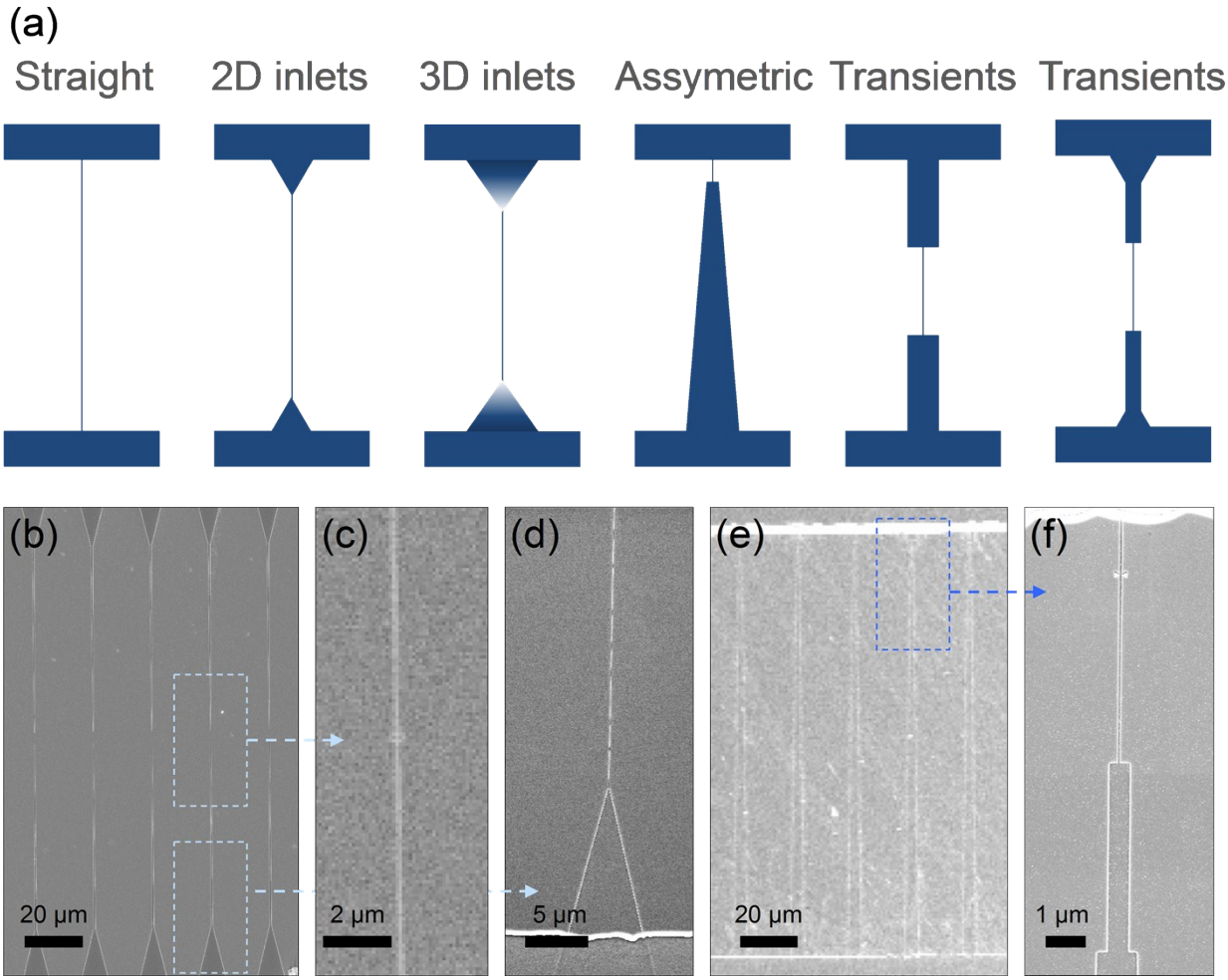

Figure S 4. Different configurations for contacting the nanochannels. Sketch (a) and SEM images of some of the stamps and samples fabricated for this work (b-f). Some samples had long, straight nanochannels. Other had triangular inlets to connect them to the microchannels, as shown in (b-d) for 2D inlets. Figure S 3 shows two devices with 3D inlets. We also fabricated non symmetrical structures, where the nanochannels were connected directly to the microchannel on one side, and had transient nanochannels (larger cross section and some times also depth) on the other, as shown in (e,f). We also fabricated devices with transient nanochannels with different depths, as shown in Figure S 5.

Figure S 5 shows a general overview of a device with short nanochannels, transient nanochannels and 3D tapered inlets. In (a) the microchannels, the triangular tapered inlets, and the transient nanochannels can be seen. (b) shows a detail of the transient nanochannels, connecting the nanochannels with the antenna, in between the two transient parts, as shown in (c). The nanochannels, some as small as 30 x 30 nm, are not visible in the optical images, and can just be visualized by SEM. The SEM images in (d) show different nanochannels from the device, with their corresponding nanoantenna.

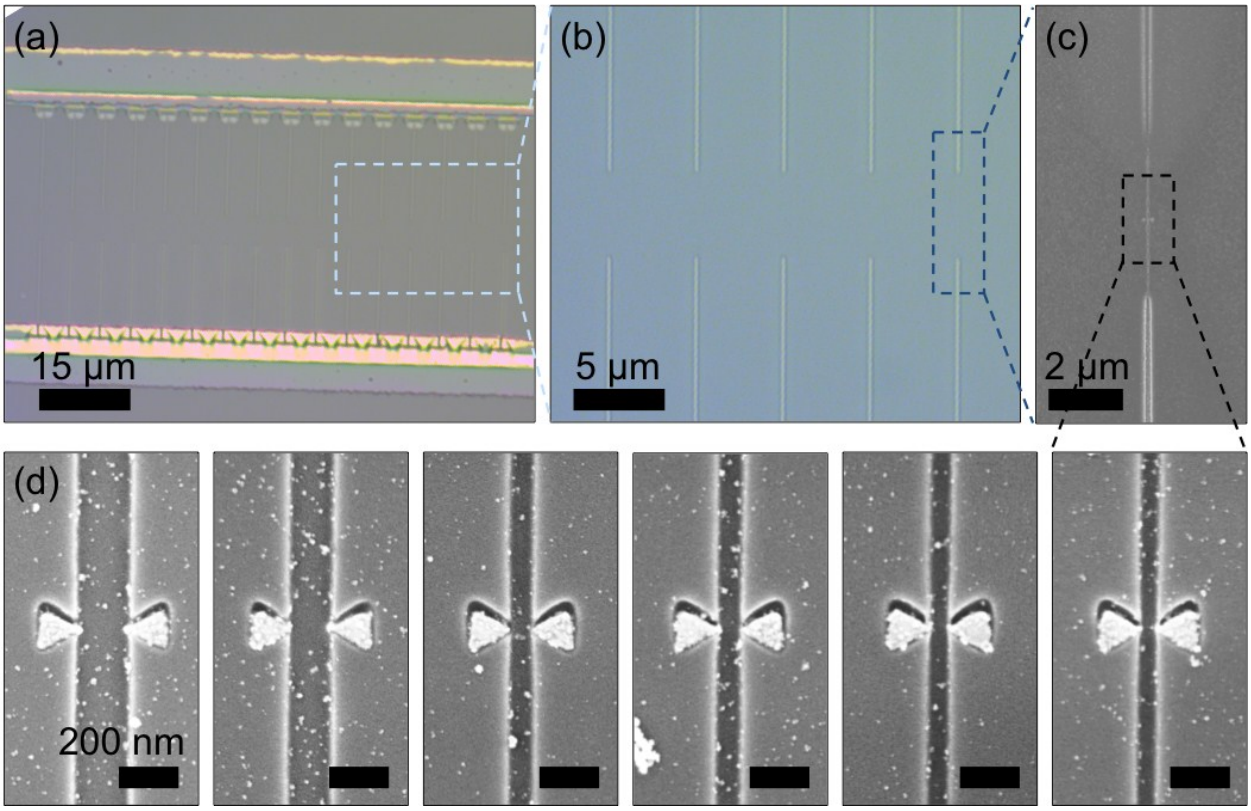

Figure S 5. Overview of one of the devices after gold lift off. The microchannels, the inlets, transient nanochannels and nanochannels can be seen. (a) Optical image with a general overview. (b) detail of (a), where the transient nanochannels can be seen. The nanochannels are in the center, although hardly visible. (c) shows the transient nanochannels and the nanochannels with the nanoantenna in the center. (d) shows different nanochannels with their corresponding antenna, with variable width and gap.

S2. Fluidic performance

S2.1 General flow

Different liquids with different fluorophores were flown into the device for general flow tests. Figure S 6 (b)-(f) show a representative example of how the liquid (Isopropanol with Alexa Fluor 645) flows from the top microchannel along the nanochannels, and then fills the microchannel at the bottom. There are 12 different nanochannels in this device, as schematized in (a), although they cannot be seen with the 20x objective used for these images given they small dimensions. The triangular tapered inlets at the entrance and exit of each nanochannel can be clearly seen, and the liquid accumulation observed before they wet

the microchannel. They nanochannels have different cross-sections: the widest ones are at the sides, and are 150 nm wide, 30 nm deep. Then the width is gradually reduced, down to 25 nm wide corresponding to the two nanochannels at the center. They are all 30 nm deep and 150 µm long. It is clearly seen how the liquid flows faster along the wider ones, and needs more time to wet the smaller ones. The images are a combination of fluorescence and bright field, to facilitate the visualization of the fluidic structures.

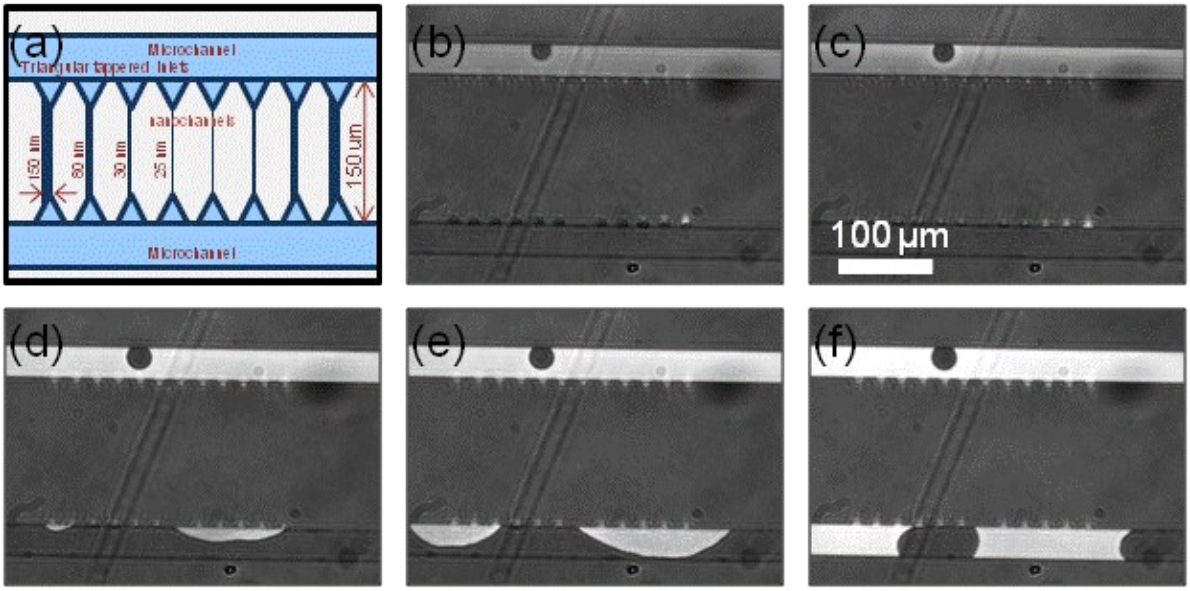

Figure S 6. Flow of liquid from the top microchannel down to the bottom one, passing along the 12 different nanochannels with different lateral sizes. A sketch is shown in (a), with the spatial distribution of the micro and nanochannels. The fluorescence images (b)-(f) are combined with brightfield, for easier structure visualization.

Visualization of such small nanochannels in a fluorescence microscope is very challenging. The liquid needs a very high concentration of fluorescent dyes so the 30 nm x 30 nm nanochannels can be seen, even when using a high sensitivity (EM-CCD) camera. But, such high concentrations give extremely high signals in the microchannels (20 µm x 1 µm), so the whole image is saturated from such high intensities, making the observation of the nanochannels impossible. In the microscope used to acquire the images in Figure S 6, we did not have the option to physically reduce size the excitation spot, when the nanochannels are illuminated, so are the microchannels. For these reasons, most of the fluorescence images of this work were obtained by confocal (laser scanned) microscopy. Here, the excitation spot is limited by diffraction, but it is orders of magnitude smaller than in the wide field microscope. This means that when the nanochannel is excited, the microchannel is not, so the detector does not get saturated. This way, we can observe the flow of liquids stained with fluorescent dyes as they flow along the nanochannels.

S2.2 Leaking detection

The quality of the sealing and the confinement of the liquid into the nanochannel was confirmed by spatially resolved spectroscopy. We acquired the fluorescence spectra at different spots of the sample in a

confocal (laser excited) microscope. The laser was focused down to a 600 nm diameter spot, and placed at different areas of the sample; then, the signal was recorded to make an image, or the spectrum of points of interest was acquired using a spectrometer. Figure S 7 (b) and (c) show two confocal, photoluminescence images obtained with a laser excitation of 532nm, for a channel filled with an aqueous solution of Rhodamine 6G (λ_{ex} = 525 ; λ_{em}= 547 nm) where an inlet (c) and a nanochannel (b) can be seen. An intensity profile across the nanochannel is shown in (a). The spectra of the photoluminescence signal obtained at different points was measured. (d) is the spectrum of the signal from the nanochannel, where the fluorescent peak of the Rhodamine at λ = 547 nm can be seen. (e) is the signal from the background, where hardly any signal can be observed. And (f) is the signal from the inlet, where the same fluorescence peak as that in (d) can be seen, with a higher intensity, since the inlet can fit much more liquid inside.
The spectra from the background was obtained just few microns away from the nanochannel. This proves that the bonding and the sealing are very good and that there is no liquid leakage outside the fluidic structures.

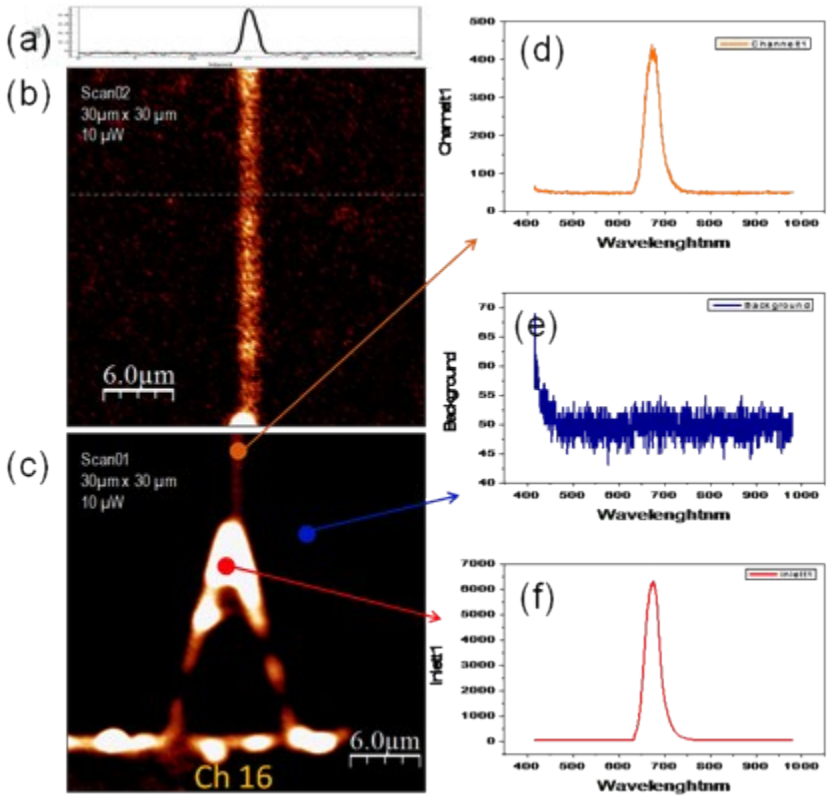

Figure S 7. Confocal spectroscopy to check the quality of the sealing. Confocal images of two different areas of the sample are shown: (b) corresponds to a nanochannel, and (c) to a tapered inlet. (a) is an intensity profile along the nanochannel shown in (b). Three photoluminescence spectra from three different spots are shown in (d), (e) and (f), corresponding to the nanochannel, the background, and the inlet respectively.

S2.3 Flow of DNA molecules in the nanochannels

We observed a successful flow of liquids along the nanochannels in most of the cases, even for the nanochannels with the smallest cross sections (27 nm x 30 nm). We took advantage of such small nanochannels to flow and stretch single molecules of DNA. DNA is usually coiled, but can be stretched into confined structures - almost to its total countour lenght when the effective size of the channel is close or smaller than the gyration radius of the molecule.

In this work, we used λ-DNA stained with YOYO-1, in a ratio of 5:1 basepairs per dye. At this staining ratio it has a contour lenght of L_λ = 21.8 µm. The DNA was diluted in a TBE/TAE buffered solution, to have a concentration of 100 ng / mL. The molecules were driven into the nanochannels by electrophoresis. A voltage difference (80V) was applied between the two opposite microchannels, so the molecules were forced to flow through the nanochannels. Figure S 8 (a) shows a wide field fluorescence microscopy image, where different DNA molecules stretched along different nanochannels of the same device can be seen.

Profiles of single molecules along the nanochannels with different cross-sections can be seen in Figure S 8 (b) - (d).We measured a stretched length L_s = 18.7 µm for the 30 x 27 nm^2 (Figure S 8 (b)), which gives a stretching value of L_s/L_λ=0.89, approaching the total contour length of these molecules. This value is higher than those reported for channels of similar sizes made of glass. We attribute this to the negative charge on the polymer nanochannels walls, which creates a higher repulsion (the molecules are also negatively charged) and elongates the DNA more than when the surface has lower charge.

Nanochannels with wider cross sections do not show such a high confinement (Figure S 8 (c) and (d)).

A video showing the molecules stretched in and passing through the channels is attached to the article.

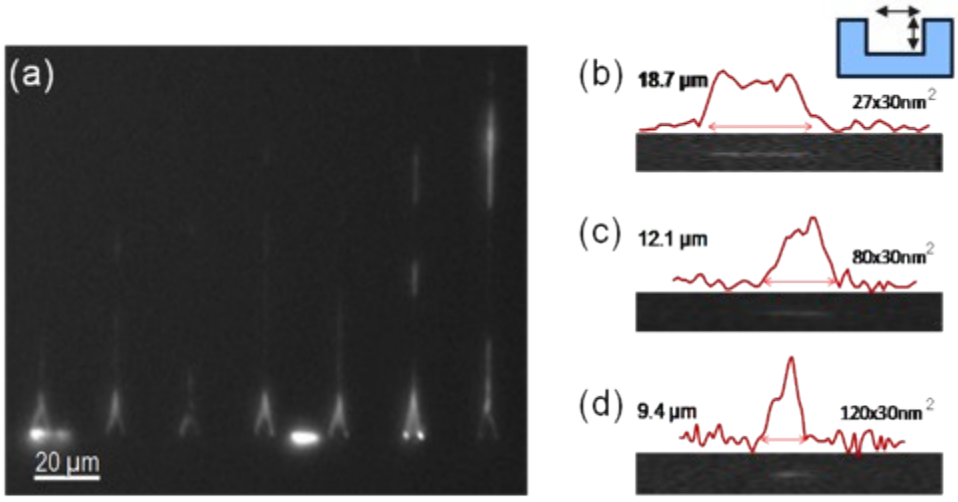

Figure S 8. DNA single molecules, stretched along the nanochannels. (a) Fluorescence image of several molecules along different nanochannels with different cross sections from the same device. (b), (c) and (d) show the fluorescence image of molecules and their corresponding intensity profiles for different nanochannel cross sections: 27 nm x 30 nm in (b), with a stretched lenght of 18.7 µm. 80 nm x 30 nm in (c), with a lenght of 12.1 µm. And 120 nm x 30 nm in (d), with a lenght of 9.4 µm.

S3. Optical performance of the antenna

The two photon photoluminescence (TPPL) signal was measured at the antenna, and at a non-structured gold surface to quantify the signal enhancement given by the plasmonic effect.

A laser (Ti:sapphire laser, τ =120 fs, λ=830 nm) was focused to a diffraction-limited spot on the bowtie-air interface using a 0.95 numerical aperture (N.A.), 100x objective. Gold TPPL was collected by the same objective and passed through a band-pass filter to transmit only wavelengths between 460 and 700 nm. The luminescence signal was recorded by a single-photon counting avalanche photodiode for signal quantification. Figure S 9 shows a TPPL image of a bowtie nanoantenna with a nominal gap of 35nm, excited by an incident polarization parallel to the bowtie axis in (a) and with the perpendicular polarization in (b). The signals strongly depends on incident polarization, evidence that the TPPL is a result of field enhancement due to triangle-triangle coupling. The excitation is 100 times greater than for perpendicular polarization. TPPL of a bowtie with a gap of 200 nm has a signal intensity significantly lower. These observations demonstrate that the coupling decays for triangles at this large gap. Field enhancement is still observed from single metallic triangles due to their sharp tips, but to a much lesser degree than that from coupled pairs. To directly determine optical field enhancements, the TPPL signal of non-structured gold films from the same sample were measured as comparison. Figure S 9 (c) is a TPPL image from a non-structured gold film few microns away from bowties, to ensure that the quality of the metal and the thickness are exactly the same as for the bowtie nanoantennas. In this case, the intensity of the laser was increased in 25 times, to have a comparable signal to that from the nanoantenna. The TPPL intensity profiles are shown in the graph of Figure S 9 (f) for the smooth gold film (black line), and the 35 nm gap bowtie antenna for the two different polarizations (red and green lines). If we assume that no field enhancement occurs in the flat film, then an enhancement in the metal of bowtie α can be calculated from the ratio of TPPL intensities from the bowtie and the film. This ratio is given by equation S1,

$$\frac{\langle TPPL_{bowtie} \rangle}{\langle TPPL_{flatAU} \rangle} = \frac{A_{bowtie}}{A_{flatAU}} \alpha^2 \frac{\langle P_{bowtie} \rangle^2}{\langle P_{flatAU} \rangle^2} \qquad \text{(S1)}$$

where $\langle TPPL_{bowtie} \rangle$ is the (time averaged) TPPL signal when the laser is focused at the bowtie, $\langle TPPL_{flatAU} \rangle$ is the TPPL signal when the spot is focused at the Au film, $\langle P_{bowtie} \rangle$ is the average incident power at a bowtie that gives $\langle TPPL_{bowtie} \rangle$, $\langle P_{flatAU} \rangle$ is the average incident power at the film that gives $\langle TPPL_{fiatAU} \rangle$, A_{bowtie} is the surface area of the bowtie from which the $\langle TPPL_{bowtie} \rangle$ was measured, and A_{flatAU} is the total surface area of the Au film from which the $\langle TPPL_{flatAU} \rangle$ was measured.

We assume the area A_{flatAu} excited by the focused laser is equal to a circular region with a diameter equal to the full width at half maximum (FWHM) of the laser spot. For λ= 830 nm and NA= 0.95, the measured FWHM from a diffraction-limited TPPL spot is around 600 nm, so A_{flatAU} = 282 000 nm^2. Since the measured antennas have typical dimensions in the range of 100 nm wide x 100 nm long, an enhancement in the order of $\alpha^2 = 10^4$ was obtained.

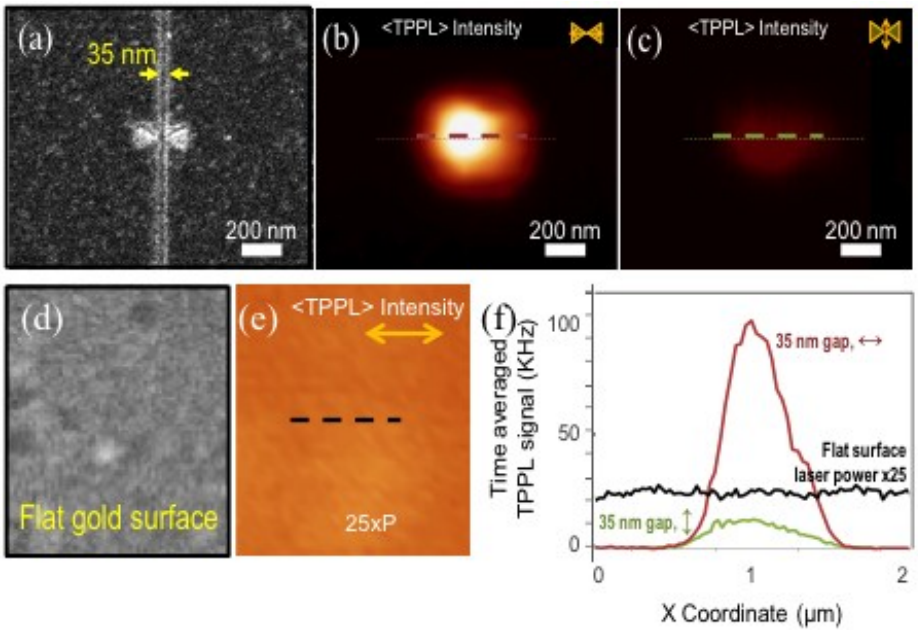

Figure S 9. Two photon photoluminescence (TPPL) characterization. (a) shows the SEM image of a 35 nm gap gold antenna. (b) and (c) show the TPPL images of this antenna depending on the polarization: when excited with the electric field parallel (b) and perpendicular (c) to the main antenna axes. (d) shows a SEM image of a flat, non-structured gold surface on the same sample. (e) shows an image of the spatial TPPL intensity distribution on this area, with a much weaker signal. The intensity scale is the same in (b) (c) and (e), but the image of the flat gold surface shown in (e) was recorded with a laser power 25 times higher. The graph in (f) compares the intensity profiles for the three different cases: the intensity profile of the signal on the antenna with parallel (red line) and perpendicular (green line) polarizations, and on the flat surface with a 25x higher laser power.

S5. Molecule population of the optical spot for different fluidic systems

The main limitation for optical detection of single emitters or molecules is given by the number of them populating the excited volume.

- A focused laser spot illuminating a non-confined liquid sample, or a large microfluidic channel (width and depth, both > 1 μm) (main text, Figure 1 (a)), excites a volume on the order of 10^{-15} L. To reduce the excited volume, it is possible to confine the liquid into a small fluidic channel and/or reduce the illumination spot.
- A nanoslit with lateral dimensions still in the micron range, but vertical dimensions in the nanometric range, reduces the volume down to 10^{-17} L (main text, Figure 1 (b)). This is similar to a total internal reflection fluorescent (TIRF) microscope, where the illuminated volume is confined to the sample's surface.
- A squared nanochannel with 100 nm lateral dimensions would represent a further reduction in one more order of magnitude (10^{-18} L) (main text, Figure 1 (c)).
- And, in this work, we go one step further and confine also the light integrating the nanochannel with a plasmonic antenna (main text, Figure 1 (d)) into 10^{-20} L; this is five orders of magnitude smaller than the initial diffraction limited spot.

Table S 1 shows a summary of the typical excited volumes for different systems, ranging from a large microchannel down to nanochannels with different dimensions and a nanochannel integrated with a bowtie nanoantenna as explained above. And the volume reduction that they represent, compared to the non-confined case (diffraction limited spot). In addition, we have calculated the number of quantum dots that would be excited in the different configurations for the concentration used in this work (25 mg / mL). The difference goes from 2676 quantum dots for the non-confined case down to less than 1 quantum dot for the antenna nanochannel system. We also show what would be the maximum concentration (how much the sample needs to be diluted) to guarantee that there is just one emitter at the time in that spot.

	System dimensions		Excited volume		Volumen reduction (V_{laser}/V_{excitd})	Number of Excited QDs	Maximum [C] of QDs (mg/mL)
	Width (nm)	Depth (nm)	(nm^3)	(L)			
Laser Spot (He:Ne)	812	1639	$8.51 \cdot 10^8$	0.85 fL	1	2700	0.009
Microchannel	1000	1000	$8.51 \cdot 10^8$	0.85 fL	1	2700	0.009
Nanoslit	1000	100	$5.10 \cdot 10^7$	50 atto L	16	163	0.153
Nanoslit	1000	30	$1.56 \cdot 10^7$	15 atto L	55	49	0.511
Nanochannel	100	100	$8.13 \cdot 10^6$	8 atto	105	26	0.978
Nanochannel	100	30	$2.44\ 10^6$	2 atto	350	8	3.261
Nanochannel	30	30	$7.32\ 10^5$	700 zL	1160	3	10.870
Nanoch.+Antenna	30	30	$2.70\ 10^4$	27 zL	31500	>1	294.52

Table S 1. Dimensions and total focal volume for a laser spot and a laser spot illuminating different fluidic structues: a large microchannel, nanoslits and nanochannels with different lateral dimensions, and a nanochannel with a plasmonic antenna (plasmonic hot spot). The *dimensions* used for each system are listed on the table. The calculated excited volume for each one, both in nm^3 and L are shown. The rate of the reduction in the focal volume compared to the laser spot has been calculated, as well as the number of quantum dots (QDs) present in there for a 25 mg/mL concentration. The last column shows the maximum concentration where single quantum dot detection would be possible (to guarantee that the concentration is so low that only one QD would be present in the excited volume).

S6. Detection of quantum dots - Data analysis and statistics

S6.1 Antenna localization

We have used a home made set up, with a piezoelectric stage, synchronized to a single photon counter, to obtain the light intensity with spatial resolution by scanning a laser over the sample surface. Using an adequate set of filters, we can filter out the laser signal and record only the fluorescent signal scattered and/or emitted by the quantum dots. Figure S 10 shows an example of the image obtained with the self built confocal microscope, by scanning a 633 nm laser over the fluidic device. In (a) a low magnification image is shown, where four different transient nanochannels, 150 nm x 150 nm can be seen. These connect the nanochannels (30 nm x 30 nm, 5um long) and the antenna to the microchannels. In (b), a detail of the antenna/nanochannel system is shown.

Once the exact position of the antenna (bright spot in (b)) and the nanochannels has been found, the laser is placed at the desired spot using the piezoelectric stage, to ensure maximum accuracy. And then the photoluminescence signal from that specific point is recorded with a single photon counter, as shown in (f) for the laser placed at the antenna or at the nanochannels. To improve the spatial resolution and minimize the noise, we use a confocal pinhole (100 um diameter) at the output. This pinhole, combined with the 100x objective used for imaging, guarantees not only that we collect signal from the focal plane, but also limits the spatial collection of light down to a 1um spot.

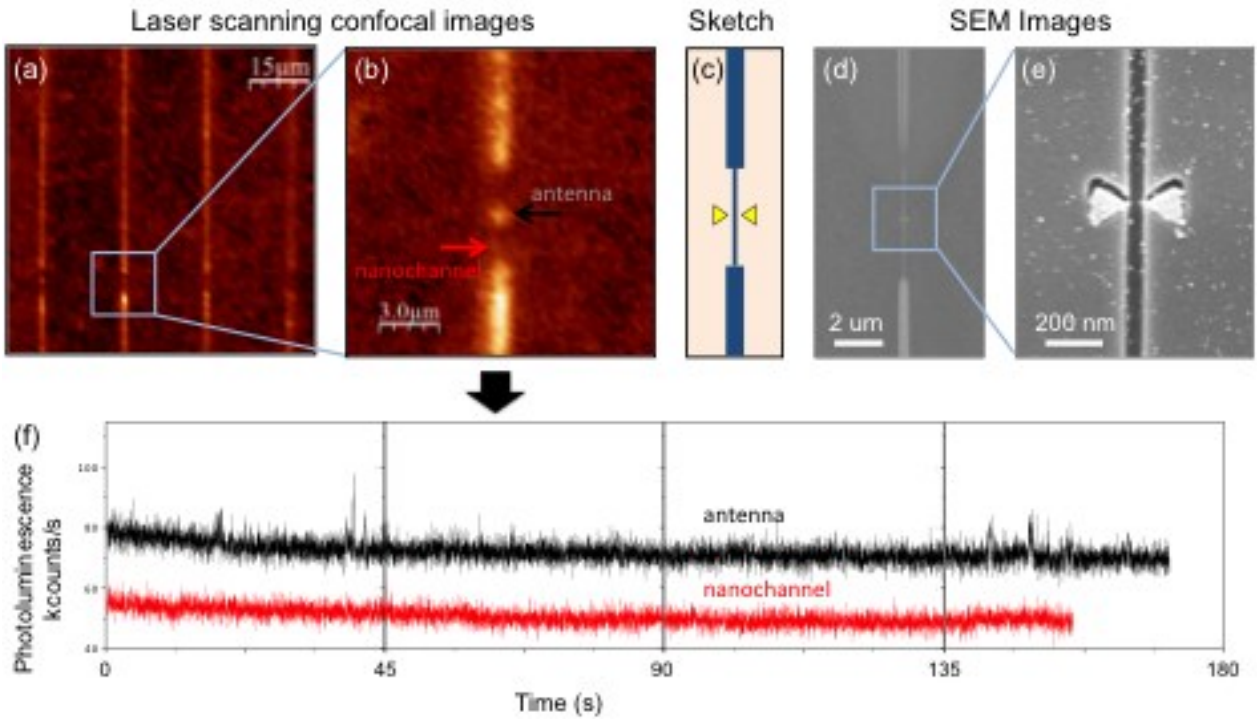

Figure S 10. Topography signal to localize the antenna and the channel prior to the measurements. The SEM images do not correspond to the exact same device, but to a similar, representative one. The samples used for fluidic and optical measurements were only imaged after the measurements, to avoid carbon contamination and modification of the optical properties of both, the gold and the polymer.

S6.2 Raw data

Figure S 11 shows two representative time scans obtained by focusing the laser spot (λ = 633 nm, P = 40 μW) at different positions of the same nanochannel: at a bare segment of the nanochannel (blue line) and at a segment of the nanochannel with a plasmonic antenna (red line). Both signals are compared against the same background (black line), obtained by exciting a flat polymer spot in the vicinity of the nanochannel, which has no flow. All three time scans (antenna, channel and background) were obtained on the same sample and same nanochannel just by moving the laser position few microns with a piezoelectric stage. The typicall duration of the scans is one or two minutes, and the number of particles that pass trough depends on their concentration. We measured on different nanochannels on the same device, and also on different devices, all with similar characteristics, and obtained comparable results.

And we used two different types of quantum dots with different composition and solubility: cadmium free quantum dots, made of CuInS/ZnS, suspended in toluene and CdSe quantum dots with a polymer coating, suspended in water. The results are comparable for both types of nanocrystals. We recorded time scans with different laser powers. Similar analysis was done for each one of them. New backgrounds were recorded for each nanochannel and each laser power.

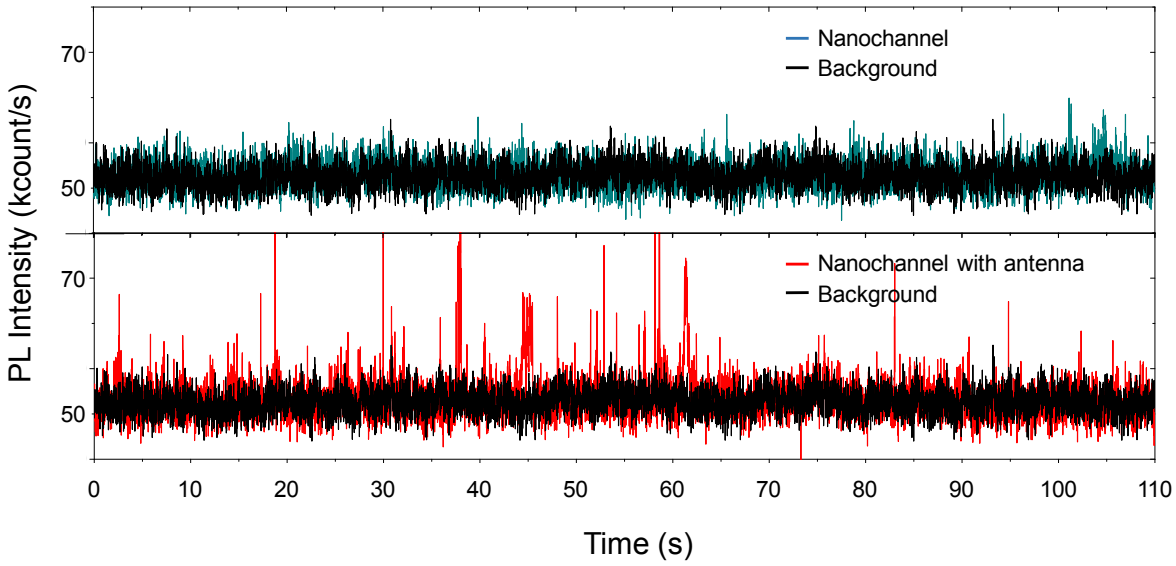

Figure S 11. PL data obtained from the Photoluminescence time scans, from a diffraction limited spot in a nanochannels (top graph) and from a plasmonic hot spot in a nanochannels (bottom graph). Both signals are compared against the same background, obtained on a flat polymer spot in the vicinity of the channel.

S6.3 Histograms

A histogram was plotted for each time scan to study the intensity distribution of the signal. Figure S 12 shows the histogram of the time scans of Figure S 11 for the background signal (a), the nanochannel (b) and the nanochannel with antenna (c), together with their corresponding Gaussian fits (black lines). Table S 2 shows the fitting parameters obtained for the gaussians. The nanochannel and the background have similar widths, while the antenna has a broader distribution, since also the background signal is affected by the plasmonic antenna.

Figure S 12 (d)-(f) show the detail of the region of interest of the three plots in (a)-(c). Here it can be seen how the scan at the plasmonic hot spot shows a large number of peaks that have an intensity clearly higher and distinguishable from the background. This is different for the nanochannel scan – there are some peaks with intensities above the background, but there are some that are below. This can be seen as a shoulder in the histogram, compared to the Gaussian fit. This makes the particle detection very difficult for this excitation power without the plasmonic antenna. With this analysis, we established an intensity

threshold (for example, 60 counts for this specific laser power of 40 uW), what is important for the quantification of nanoparticles, as described in the main text.

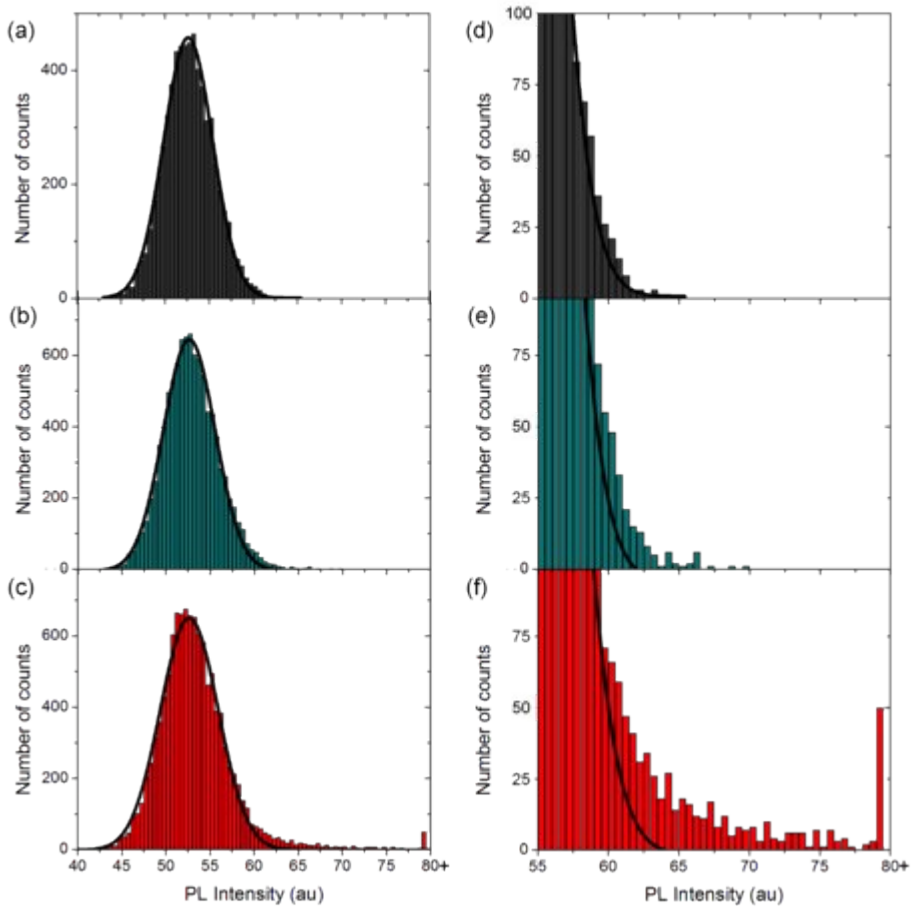

Figure S 12. Histograms for the intensity of the three time scans of Figure S 11: for a flat polymer surface (i.e., background) (a), for a nanochannels (b) and for a nanochannels with an antenna (c). A zoom of the high intensity distribution (I>55 counts) is shown in (d-f) for each case respectively. The total number of sampling points for the background histogram is n=6291, n=9628 for the nanochannel and n=11192 for the bowtie.

	Xc	w	FWHM
Background	52,60±0,04	5,55±0,13	6,53 ± 0,15
Channel	52,59±0,04	5,81±0,11	6,85±0,13
Antenna	52,64±0,05	6,37±0,16	7,50 ±0,18

Table S 2. Parameters obtained for the Gaussian fit of each graph: center of the peak (Xc), half width (w) and full width at half maximum (FWHM).

S6.4 Detection of quantum dots: Peak analysis

After establishing the intensity threshold, we did a detailed peak analysis. Figure 6 (a) and (b) in the main text show two exemplary peaks, for the nanochannel and the same nanochannel with a plasmonic bowtie antenna respectively. Several of these peaks can be seen in the time scans in Figure S 13**Figure S** . The peaks from the nanochannel are typically longer and low in intensity, while those obtained from the hot spot are sharp and shorter. A careful look at the PL peaks obtained from the plasmonic antenna reveals that the sharp peaks appear imposed on another peak, longer and weaker. This "base peaks" are very similar to those obtained without the nanoantenna, and correspond to the emission from the diffraction limited laser spot.

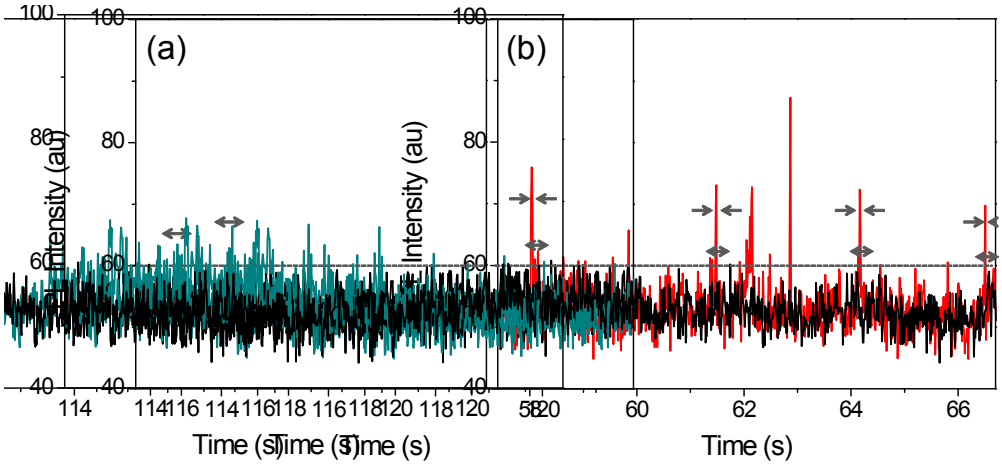

Figure S 13. Signal from a quantum dot in the nanochannel and in the nanochannel but enhanced and confined by the antenna.

S6.5 Peak Duration

In the main text, a detail analysis of the PL peaks obtained as the quantum dots flow trough the laser spot with and without antnenna is shown. Scattering plots are shown in Figure 5 in the article, and histograms showing the intensity distribution for different excitation intensities in Figure 6.

For a detailed analysis of the time duration of each peak (i.e., how fast the quantum dots travel along the nanochannels), Figure S 14 shows the histograms for the peak duration obtained from the signals measured for different laser powers. From these histograms it can be seen that there is a big dispersion in the data. This makes it more difficult to extract a value for the typical peak duration for the different laser powers.

What is clear from the graphs is that most of the peaks have a duration in the range of 15 / 20 ms. The exact peak position and the data dispersion is different is different for each set of measurements obtained with different laser powers. This probably indicates that there are two competing effects: trapping, due to the high optical fields, and increased flow, due to heating effects. For the higher laser powers (65 uW and 125 uW), the distribution is centered around the fast peaks, indicating that the flow is fast, as expected.

In the histograms it can also be seen that there are some much longer peaks; these correspond to agglomerates of quantum dots, passing one after the other, stuck together, along the antenna gap.

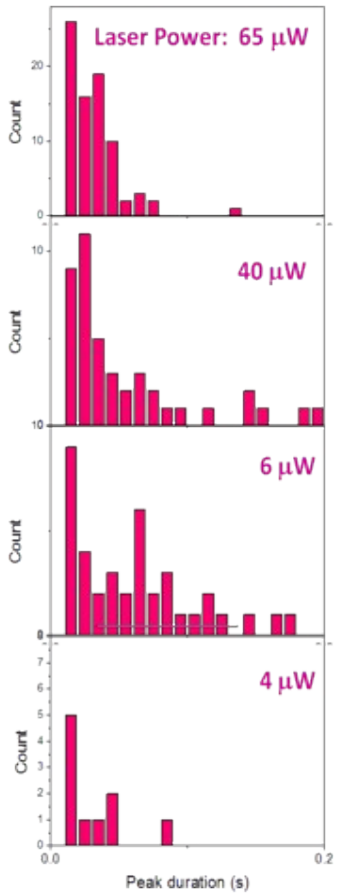

Figure S 14. Histograms showing the distribution of the duration of the PL peaks obtained for different laser powers exciting the nanochannels/nanoantenna system.

Supplementary Media

Movie 1: Lambda-DNA flowing along nanochannels. Single molecules can be observed.

References

[1] Fernandez-Cuesta, I., et al., *Fabrication of fluidic devices with 30 nm nanochannels by direct imprinting.* Journal of Vacuum Science & Technology B: Microelectronics and Nanometer Structures, 2011. **29**(6): p. 06F801.

[2] Arne, S. and S. Helmut, *Fabrication of 3D nanoimprint stamps with continuous reliefs using dose-modulated electron beam lithography and thermal reflow.* Journal of Micromechanics and Microengineering, 2010. **20**(9): p. 095002.